Experimental study of n-decane decomposition with microsecond pulsed discharge plasma

Feilong SONG (宋飞龙)[1], **Di JIN** (金迪)[1], **Min JIA** (贾敏)[1], **Wenwen WEI** (魏雯雯)[2], **Huimin SONG** (宋慧敏)[1] **and Yun WU** (吴云)[1,3,4]

[1] Science and Technology on Plasma Dynamics Laboratory, Air Force Engineering University, Xi'an 710038, People's Republic of China
[2] State Key Laboratory of Multiphase Flow in Power Engineering, Xi'an Jiaotong University, Xi'an 710049, People's Republic of China
[3] Science and Technology on Plasma Dynamics Laboratory, Xi'an Jiaotong University, Xi'an 710049, People's Republic of China

E-mail: wuyun1223@126.com

CrossMark

Abstract

A highly-integrated experimental system for the plasma decomposition of fuels was built. Experiments were conducted in a flow reactor at atmospheric pressure and confirmed that n-decane could be cracked by large-gap dielectric barrier discharge under the excitation of a microsecond-pulse power supply. Alkanes and olefins with a C atom number that is smaller than 10 as well as hydrogen were found in the cracked products of n-decane (n-$C_{10}H_{22}$). The combination of preheating and plasma decomposition had strong selectivity for olefins. Under strong discharge conditions, small molecule olefins were found in the products. Moreover, there was a general tendency that small molecule olefins gradually accounted for higher percentage of products at higher temperature and discharge frequency.

(Some figures may appear in colour only in the online journal)

1. Introduction

The continuous rotating detonation engine (CRDE) has tremendous potential for improving the performances of aero-propellers [1–3]. However, initiating the CRDE and the propagation of the detonation wave are extremely sensitive to the activity of the combustible mixture. Currently, the gas fuels such as hydrogen, acetylene, and methane can be initiated using air as the oxidant, during which the produced detonation wave can last for a certain time. For the liquid fuels such as gasoline, diesel, and kerosene, the denotation can be initiated by supplying oxygen or by using oxygen as the oxidant [4]. Transforming large molecule hydrocarbons in liquid fuels, such as kerosene, into small molecule hydrocarbons, which are much more prone to detonate has proven

to be an effective way of using CRDE in current aircrafts. Cheng *et al* proposed that olefins exceeded alkanes in laminar flame speeds, and further, the laminar combustion rates of straight-chain olefins were greater than those of branched-chain olefins [5]. Additionally, olefins have better combustion performances than alkanes at low temperatures [6]. These conclusions show direct significance of further cracking experiments from the aspect of cracked product categories.

At present, the traditional cracking methods include thermal cracking [7, 8] and catalytic cracking [9]. Of which, the thermal cracking requires a high temperature. For example, the initial cracking temperature of n-decane is approximately 900 K [8]. The catalytic cracking requires expensive catalysts [10] and always brings about catalyst poisoning [11]. By contrast, using plasma technology produces various types of high-energy particles, such as excited particles and free radicals that can theoretically react with large molecule chain hydrocarbons for

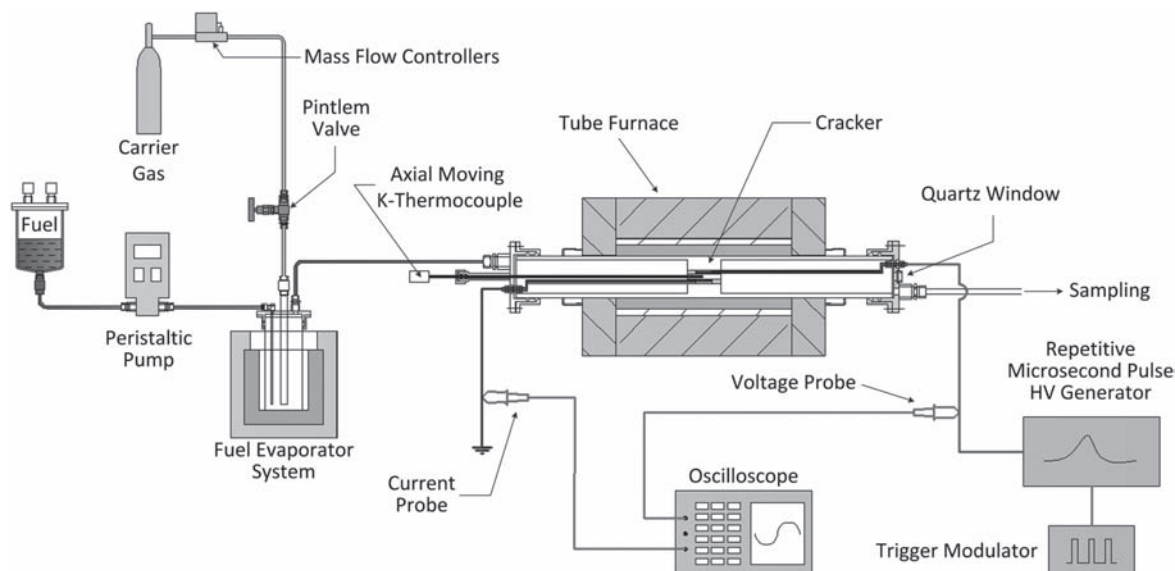[4] Author to whom any correspondence should be addressed.

Figure 1. The schematic diagram of the experimental system.

decomposition. Moreover, the chemical reaction rate can be greatly increased, and the energy consumption of the reaction can be effectively reduced [12]. Therefore, this novel method of fuel molecules decomposition using plasma has received much attention. Wang *et al* [13] used synchrotron vacuum ultraviolet ionization mass spectrometry and detected the decomposition products of iso-propyl alcohol under the action of plasma and found a great number of free radicals and reactive intermediates. Yao *et al* [14] processed n-$C_{10}H_{22}$ using coaxial dielectric-barrier discharge (DBD) with a discharge gap of 2.6 mm and small molecule hydrocarbons were detected in the products. Prieto *et al* [15] adopted a parallel-plate electrode for processing static heavy oils and detected a great amount of hydrogen as a result of long retention time. Yu *et al* [16] used Ar plasma to process heavy oils and produced a lot of gaseous hydrocarbons including hydrogen, methane, and ethylene, of which a large proportion was methane. Tsolas *et al* [17] conducted both pyrolysis and plasma decomposition on C_1–C_4 alkanes and heptane, which shows that plasma decomposition remarkably reduced the initial decomposition temperature. However, they did not focus on the decomposition of large molecule chain hydrocarbons.

To more closely approximate practical engineering applications, the parallel-plate DBD with a discharge gap of 6 mm was used in this study. N-decane is an important component in aviation kerosene and is generally used in monocomponent or multi-component alternative fuels [18–20]. Thus, in this study we performed plasma decomposition of n-$C_{10}H_{22}$ to examine the combined decomposition of preheating and plasma on the selection of products.

2. Experimental

Figure 1 illustrates the set-up of the experimental system, which consisted of a gas generator, a power supply, an electrical characteristics testing part, and a plasma cracking reactor. Using a digital peristaltic pump (BT300 M) equipped

with a 10-roller pump head, n-decane (with a purity of 99%, Huaxia, Chengdu, China) was directed into the vaporizing chamber via a drainage pin. During drainage, the vaporizing chamber remained at 200 °C, the flow rate was 0.174 ml min^{-1} (which was equivalent to 20 sccm in the gas phase standard state), and the flow error was smaller than 0.5%. Ar (with a purity of 99.999%) was blown into the chamber using a mass flow controller (DSN-MFC-400A) with a precision of 1%, and the flow rate was set as 980 sccm. Ar was adequately mixed with the vaporized n-decane in a vaporizing chamber with a volume up to 800 ml. The quartz tube was 380 mm long. The cracker was placed at the center of the tube furnace, which was 230 mm long. The heating length was 150 mm, and the temperature was adjustable within the range from room temperature to 1200 K. The other parts of the quartz tube remained at 200 °C by heater band. Before discharge, the temperature at the center of the cracker was measured by an axially-movable K-type sheathed thermocouple for which the outer diameter of the sheathed wire was 1.5 mm. This temperature was then adopted as the experimental temperature.

Figure 2 shows the structure of the cracker. The plasma was produced using a parallel-plate DBD. Two quartz shells were fastened with four bolts, and the α-Al_2O_3 ceramic dielectric layer (30 mm length, 30 mm width, and 1 mm thickness) was pressed against the top and bottom surfaces of the square quartz tube (1 mm wall thickness, 6 mm internal height, and 10 mm internal width) to produce a uniform plasma discharge and to avoid generating an electric arc. The copper electrode plates (20 mm long and 10 mm wide) were placed outside the dielectric layers. M3 threaded holes were drilled at the center of each quartz shell, and then the copper electrode plates were pressed against the ceramic surface using copper screws. Two copper screws were connected to a high-voltage power supply and to ground terminals with a copper screw rod. The external width of the square quartz tube was 30 mm, and this effectively prevented creepage
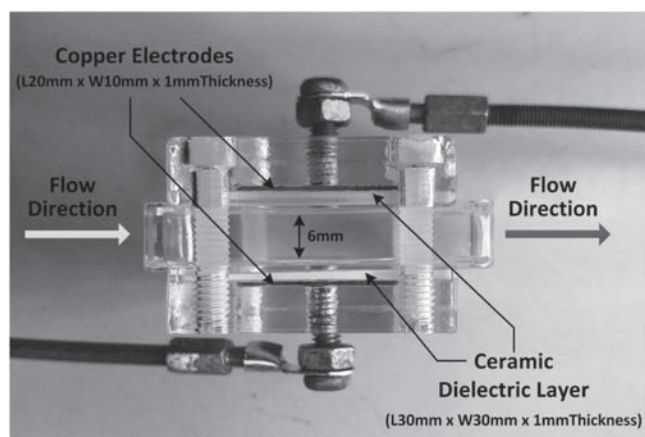
Figure 2. Picture of the DBD cracker.

between the two electrodes outside of the quartz tube. The volume of the plasma produced by the cracker was 1200 mm^3, and the gas was retained for 72 ms.

The cracker was supplied by a microsecond-pulse power supply. Figure 3 illustrates the typical voltage–current waveforms. The frequency of the microsecond-pulse power supply was adjustable within the range of 200 Hz–5 kHz, and the voltage was adjustable from 0 to 12 kV with a rise time of 1.5 μs. The discharge frequency was precisely controlled via external triggering. The discharge parameters were measured using a high-voltage probe (P6015A) and a current probe (TCP0030A). The data were acquired using a digital oscilloscope (MDO3024).

The experiments were conducted at three temperatures: 520, 640 and 750 K. At each temperature, the discharge frequency was set at 1 and 2 kHz, and the discharge voltage was set at 11 kV. For comparison, a set of experiments were conducted with a temperature of 823 K and frequency of 5 kHz. Due to the characteristics of the power supply, the voltage was 9 kV.

After air cooling, some high-temperature products from the outlet of the tube furnace condensed into liquids, and others underwent water cooling to collect the gaseous products. 1.8 μl of the liquid products were selected and injected into the instrument using a sample injection pin for component analysis. The component detector gas chromatograph (GC/MS) included a gas chromatograph (Agilent 6890-series) equipped with a chromatogram column (HP-Innowax, with a size of 30 m $\times$ 0.25 mm $\times$ 0.25 μm) and mass spectrometer (HP5973N). We acquired qualitative results using the NIST mass spectrometry database. In addition, semi-quantitive analysis was performed on a single component according to the area percentage of the total ion chromatogram in the mass spectra. 100 μl of gaseous products were taken and injected into the GC using a sample injection pin. The GC (Agilent 7890) was equipped with a molecular-sieve capillary chromatography column (PLOTC-2000, with a size of 25 m $\times$ 530 μm $\times$ 20 μm) and a thermal conductivity detector. H_2, CH_4, C_2H_4, and C_2H_6

were successfully separated. The generated gases were quantitatively analyzed using an external standard method.

3. Results and discussion

Figure 4 shows the microsecond pulse discharges with and without the injection of n-$C_{10}H_{22}$ (a kind of large molecule straight chain alkane). After the injection of n-$C_{10}H_{22}$, the discharge weakened compared to that after the injection of pure Ar. During the plasma decomposition process, high-energy electrons collided with Ar atoms in each pulse discharge breakdown, and then the Ar atoms were excited from their ground state to a metastable state. Subsequently, the metastable-state Ar atoms collided with molecules or free radicals in the gas to crack the molecules and free radicals [21, 22]. Tsolas *et al* [23] conducted related experiments and concluded that, under a high degree of dilution, decomposition induced by the direct collision between electrons and molecules contributed slightly to the consumption of the molecules. In this study, the degree of dilution of n-$C_{10}H_{22}$ was quite high in the carrier gas with a mole fraction of 0.02 under standard state. The direct collision with electrons hardly cracked n-$C_{10}H_{22}$, and the collisions with metastable-state Ar atoms dominated the decomposition of n-$C_{10}H_{22}$.

Figure 5 shows the results of the liquid products after the plasma decomposition of n-$C_{10}H_{22}$. Ar was used as the carrier gas in the decomposition process. The structure distribution of the detected products under different experimental conditions are given in table 1. C_6H_{12}, C_6H_{14}, C_7H_{14}, C_7H_{16}, C_8H_{16}, C_8H_{18}, C_9H_{18}, and C_9H_{20} were all found in the liquid products after the decomposition of n-$C_{10}H_{22}$ at 520, 640 and 750 K. Zeng *et al* [8] carried out pyrolysis experiments on n-$C_{10}H_{22}$ using a flow reactor at normal and low pressures, and Malewicki *et al* [24] performed pyrolysis experiments on n-$C_{10}H_{22}$ using a high-pressure shock tube. According to their results, the initial pyrolysis temperature of n-$C_{10}H_{22}$ was approximately 900 K, and this suggests that the decomposition products detected in this study were produced in a plasma reaction rather than in a thermal reaction. Since the bond energy continues to increase from the third C–C bond to the middle C–C bond in the chain hydrocarbon [25], the bond energy of the C_5–C_6 bond is larger in the molecule of n-decane, causing few pentyls were produced. On the other hand, boiling point of pentane and pentene are lower than that of C_5 and above components, so most of them volatilize. As a result, neither pentane nor pentene were detected in the products as indicated in table 1. Different free radicals recombined and led to the formation of isomers of some products. Moreover, the branched chains of the isomers produced in the plasma decomposition process were mainly methyls and ethyls.

To more clearly present the distribution of products after the plasma decomposition of n-$C_{10}H_{22}$, the peak areas of various isomers were added together, and the percentage of each product in the total ion chromatogram area of all products were calculated. These results are shown in figure 6. At a temperature of
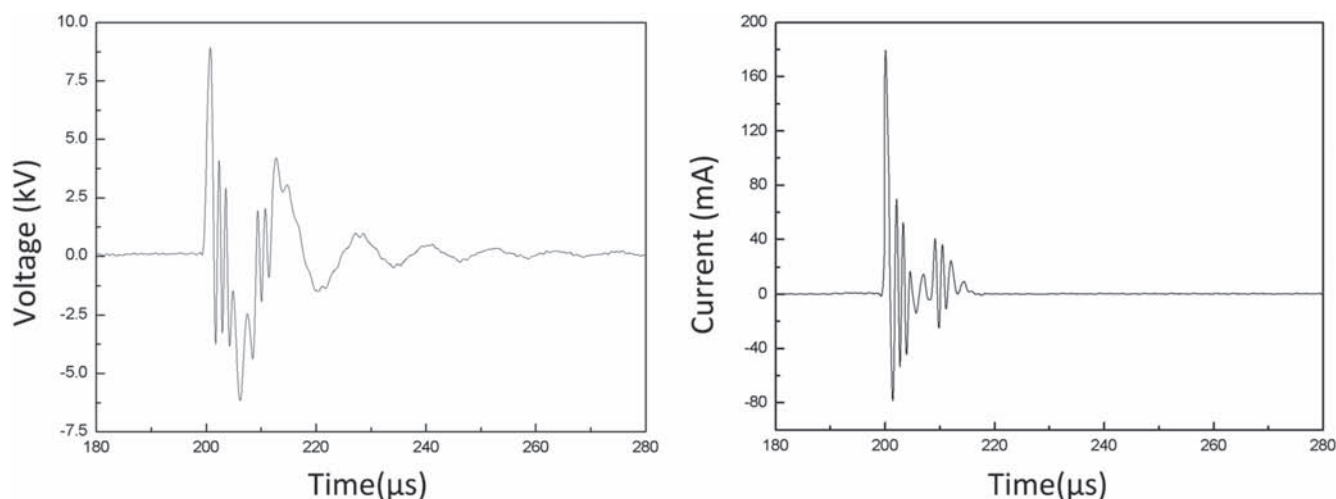
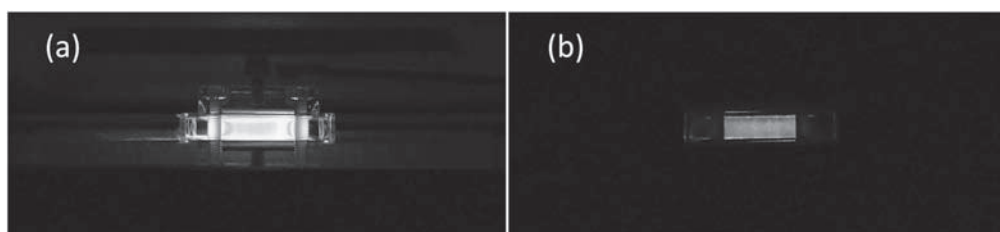**Figure 3.** Typical voltage–current waveforms during discharge.

Figure 4. Illustration of discharge from the DBD cracker at a preheating temperature of 520 K, a discharge voltage of 11 kV and a discharge frequency of 1 kHz. (a) Ar was injected at a rate of 1000 sccm. (b) Ar was injected at a rate of 980 sccm, and n-$C_{10}H_{22}$ was injected at a rate of 0.174 ml min^{-1} (or 20 sccm in gas phase).
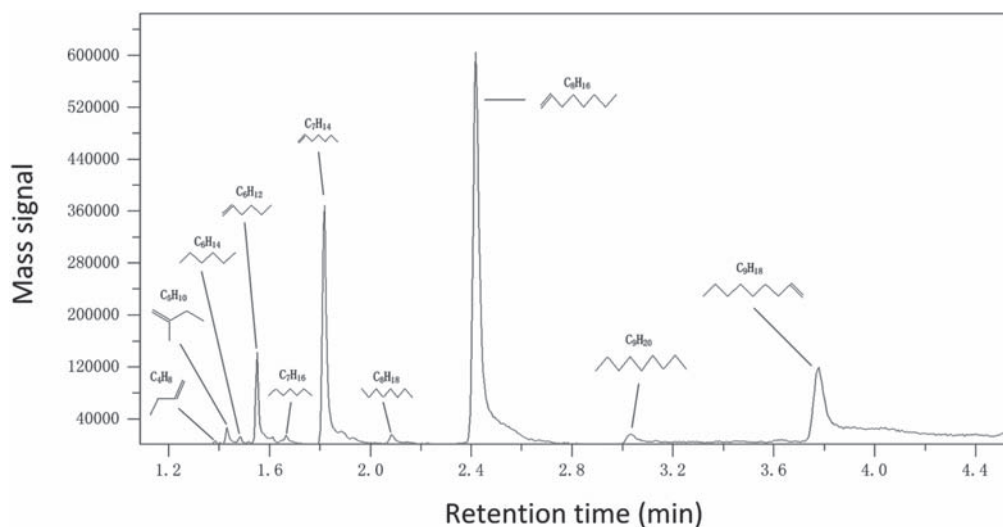

Figure 5. Typical GC-MS spectra of the liquid products of the decomposition of n-$C_{10}H_{22}$ at a preheating temperature of 823 K and a discharge frequency of 5 kHz.

520 K and a discharge frequency of 1 kHz, decomposition was insufficient because both the temperature and discharge frequency were quite low. This led to a large percentage of the large molecule alkane C_9H_{20} (as high as 38.066%) and a small percentage of small molecule olefins such as C_7H_{14}. With an increase in temperature and discharge frequency, n-$C_{10}H_{22}$ was further cracked. Thus, there was a sharp decrease in the percentage of C_9H_{20} and an increase in the percentages C_8H_{16} and C_7H_{14}. In particular, under 750 K/2 kHz, the percentage of C_8H_{16} was 79.042%, which was almost twice as great as that under 520 K/1 kHz. Moreover, the percentage of C_8H_{16} was always highest under different experimental conditions, and this can be explained by the energies of the chemical bonds. The bond dissociation energy of C–C in a straight-chain alkane is approximately 32.6–61.9 kJ mol^{-1} lower than that of the C–H bond, and the bond dissociation energy of C_2–C_3 is

Table 1. Structure distribution of products under different experimental conditions.

Products		Conditions (K kHz^{-1})					
Molecular formula	Structural formula	520/1	520/2	640/1	640/2	750/1	750/2
C_6H_{12}		√	√	√	√	√	√
C_6H_{14}		√	√	√	√	×	√
C_7H_{14}		√	√	√	√	√	√
C_7H_{16}		√	√	√	√	√	√
C_7H_{16}		×	×	×	√	×	×
C_8H_{16}		√	√	√	√	√	√
C_8H_{16}		×	×	√	×	×	×
C_8H_{18}		√	√	×	√	√	×
C_8H_{18}		√	×	×	√	×	×
C_8H_{18}		×	×	√	×	×	×
C_8H_{18}		×	×	√	×	×	×
C_9H_{18}		√	×	√	√	√	√
C_9H_{20}		√	×	√	√	√	√
C_9H_{20}		√	√	×	√	×	×
C_9H_{20}		√	√	×	×	×	√
C_9H_{20}		×	×	√	√	×	×
C_9H_{20}		√	×	×	×	×	×

Figure 6. Normalized percentages of various decomposition products of n-$C_{10}H_{20}$.

4.8–8.8 kJ mol^{-1} lower than that of the C_1–C_2 bond [25]. Moreover, the closer the C–C bond is to the center of the molecule, the greater the bond dissociation energy for octane. Thus, it is speculated that, during the collision-induced decomposition process of n-$C_{10}H_{22}$, the dissociation of the C_2–C_3 bond mainly contributed to the consumption of n-$C_{10}H_{22}$ and to the production of a great number of octyls. The dissociation of the β-C–H bond then led to the formation of 1-octylene. In addition, the olefins content in the cracked products exceeded the content of alkanes with the same number of C atoms under high temperature and frequency as seen in figure 6. The present results along with Cheng's conclusions in [5, 6], further verify the broad prospects of plasma decomposition in combustion under extreme conditions.

Figure 7(a) shows the percentages of total products, which were calculated by adding the peak area of n-$C_{10}H_{22}$ to the products ion current area. The current retention time was 72 ms, and the microsecond-pulse discharge frequency was 1 or 2 kHz. Thus, n-$C_{10}H_{22}$ underwent 72 or 144 pulses when passed through the cracker. Overall, few cracked products were produced, which only accounted for a small percentage. However, these percentages of products showed obvious regularity with the change in temperature or discharge frequency, which an increase in temperature and discharge frequency remarkably enhanced the percentages of products. For example, the total percentage of products at 750 K/2 kHz was 6 times greater than that at 520 K/1 kHz. Figure 7(b) shows the percentage of olefins in the products under different experimental conditions. In combination with figure 7(a), it was concluded that at higher temperature and discharge frequency, more cracked products were produced, and olefins accounted for an increasingly greater percentage of the products.

The percentages of alkanes and olefins under different conditions are compared in figure 8. At the same discharge frequency, as the temperature increased, the percentages of various olefins gradually increased (figures 8(a) and (c)), and the percentages of various alkanes decreased correspondingly (figures 8(b) and (d)). At the same preheating temperature, an increase in the discharge frequency resulted in a decrease of the percentage of C_9H_{18} and an increase of the percentages of C_6H_{12}, C_7H_{14}, and C_8H_{16} (figures 8(a) and (c)); for alkanes, the percentages of C_9H_{20} and C_8H_{18} dropped, but the percentages of C_6H_{14} and C_7H_{16} increased (figures 8(b) and (d)). Accordingly, it was concluded that, an increase in the preheating temperature and discharge frequency caused different effects on the percentage distributions of the products. In particular, the rise of temperature widened the differences of
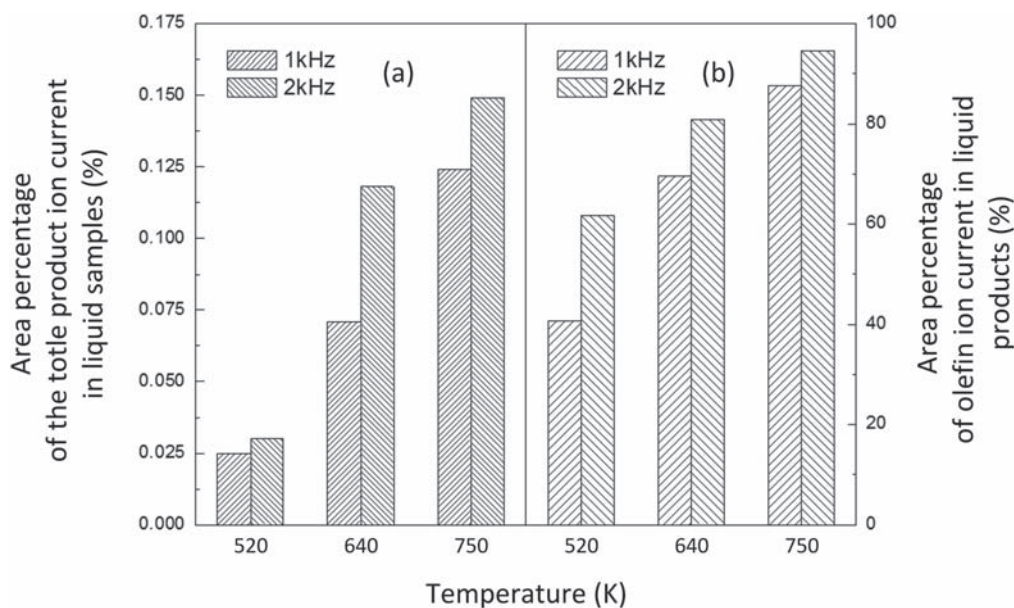
Figure 7. Under different experimental conditions. (a) Area percentages of the total product ion current in liquid samples. (b) Area percentages of olefin ion current in liquid products.
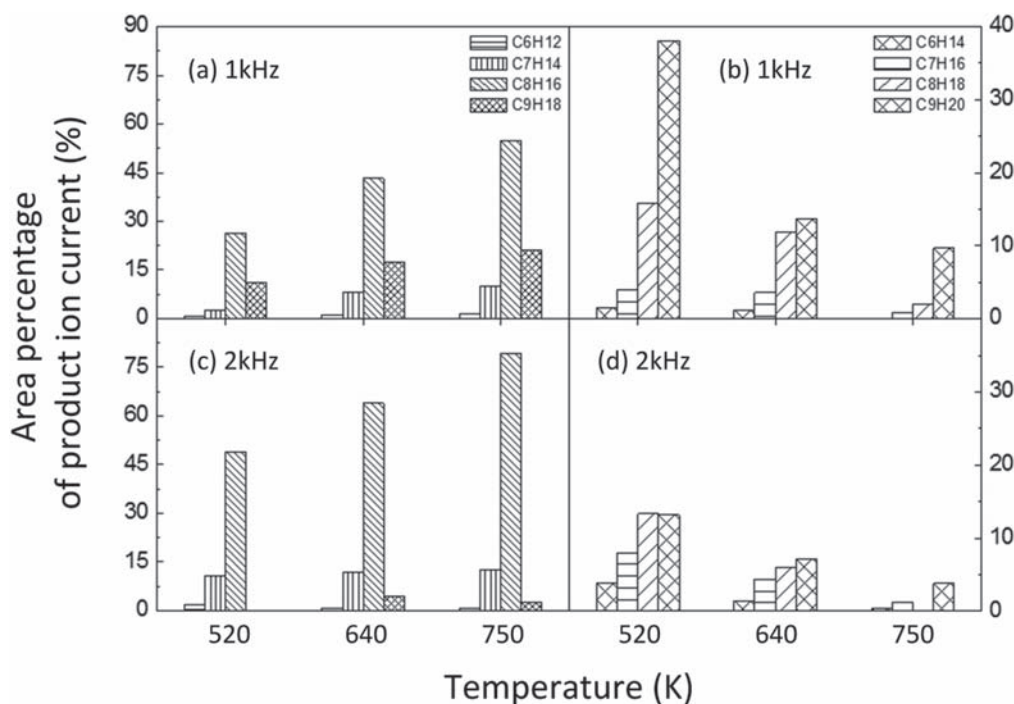

Figure 8. Percentages of different alkanes and olefins under different experimental conditions.

the percentages between alkanes and olefins, while the increase of discharge frequency enhanced the selectivity of small molecule hydrocarbon. Thus, the combination of preheating and plasma decomposition had the advantage of selectivity for small-molecular olefins.

To verify these conclusions, plasma decomposition tests were conducted at a preheating temperature of 823 K and a discharge frequency of 5 kHz. The GC-MS results of the liquid products are shown in figure 5. On one hand, the percentage of the cracked products was 0.241%, which was 61.7% higher than the value at 750 K/2 kHz, and the percentage of olefines in the

products further increased to 96.072%. On the other hand, the percentage of C_8H_{16} decreased to 54.19%, and the percentages of C_7H_{14} and C_6H_{12} increased to 20.111% and 5.93%, respectively. Additionally, some small molecule olefins, C_5H_{10} and C_4H_8, were detected. At the same time, the results of the experiments showed some tendency, with strong discharge conditions, more small molecule olefins were produced, and gradually accounted for higher percentage component in the products.

After water-cooling, the gaseous products were collected and tested using gas chromatography (7890A). Figure 9 shows hydrogen concentration under different experimental
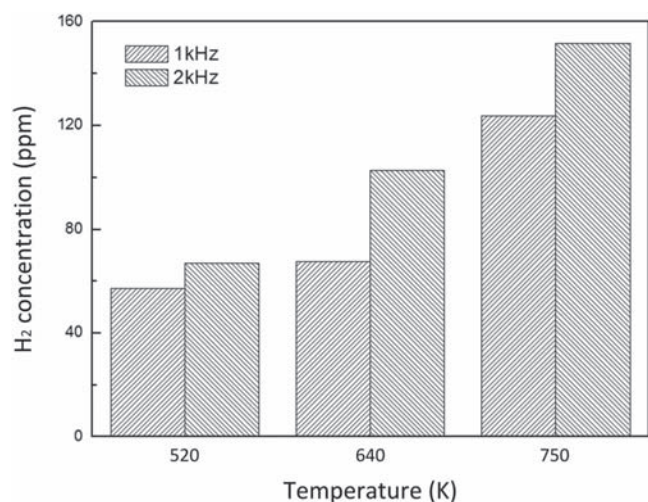
Figure 9. Effects of preheating temperature and discharge frequency on hydrogen concentration.

conditions, and it is easily seen that both the preheating temperature and the discharge frequency significantly affected hydrogen concentration. As stated above, an increase in temperature and discharge frequency led to an increase of octyl. As a result, more H atoms formed by the β-C–H bond dissociation in octyl acted as free radicals and attached to other alkyl molecules, initiating a dehydrogenation reaction and producing more hydrogen. In additional experiments, more gaseous products were detected, including H_2, CH_4, C_2H_4 and C_2H_6, in concentrations of 293 ppm, 205 ppm, 671 ppm, and 210 ppm, respectively, which the error is less than 1%. The concentration of hydrogen was nearly twice as much as that at $750\,K/2\,kHz$. Additionally, the ratio of ethylene to ethane was approximately 3.2:1. The analysis of gaseous products also verified the advantage of the combination of preheating and plasma decomposition in the selectivity of the olefins.

4. Conclusions

Plasma decomposition of n-decane was conducted using a parallel-plate DBD cracker at different preheating temperatures (520, 640, 750 and 823 K) and discharge frequencies (1, 2 and 5 kHz). The cracker was excited using a microsecond-pulse power supply, and GC and GC-MS were used to investigate the compositions of the cracked products under different experimental conditions. According to GC and GC-MS results, the direct collision between metastable-state Ar atoms and n-$C_{10}H_{22}$ led to the dissociation of C_2–C_3 bonds, and this greatly contributed to the consumption of n-$C_{10}H_{22}$. An increase in the preheating temperature and discharge frequency enhanced the production of hydrogen in the cracked products and more cracked hydrocarbons were produced, in which olefins accounted for an increasingly greater percentage in the products. Under different experimental conditions, the percentage of olefins was higher than that of

alkanes with the same number of C atoms. Varying the preheating temperature and discharge frequency caused different effects on the distribution of cracked products. Specifically, an increase in temperature widened the ratio of olefins to alkanes; at a higher discharge frequency, small molecule hydrocarbons were more easily produced. There was a general tendency that the percentage of small molecule olefins increased steadily and gradually accounted for higher percentage in products.

Acknowledgments

References

[1] Dyer R *et al* 2012 *50th AIAA Aerospace Sciences Meeting including the New Horizons Forum and Aerospace Exposition (Nashville, TN)*

[2] Welsh D J *et al* 2014 *52nd Aerospace Sciences Meeting (National Harbor, MD)*

[3] Yang C L *et al* 2016 *Exp. Therm. Fluid Sci.* **71** 154

[4] Liu S J 2012 Investigations on the structure, rotating mode and lasting mechanism of continuous rotating detonation wave Changsha *PhD Thesis* National University of Defense Technology (in Chinese)

[5] Cheng Y *et al* 2017 *Proc. Combust. Inst.* **36** 1279

[6] Cheng Y *et al* 2016 *Fuel* **172** 263

[7] Shrestha U *et al* 2015 *53rd AIAA Aerospace Sciences Meeting (Kissimmee, Florida)*

[8] Zeng M R *et al* 2014 *Combust. Flame* **161** 1701

[9] Li X F, Shen B J and Xu C M 2010 *Appl. Catal.* A **375** 222

[10] Marcilla A *et al* 2003 *J. Anal. Appl. Pyrolysis* **68** 467

[11] Cheekatamarla P K and Lane A M 2006 *J. Power Sources* **154** 223

[12] Zhang K *et al* 2016 *Trans. China Electrotech. Soc.* **31** 1 (in Chinese)

[13] Wang J *et al* 2008 *Rev. Sci. Instrum.* **79** 103504

[14] Yao S L *et al* 2016 *IEEE Trans. Plasma Sci.* **44** 2660

[15] Prieto G *et al* 2001 *36 IAS Annual Meeting Industry Applications Conf. (Chicago, IL)*

[16] Yu H *et al* 2012 *Nucl. Fusion Plasma Phys.* **32** 271 (in Chinese)

[17] Tsolas N, Togai K and Yetter R 2013 *4th Annual Review Meeting of the AFOSR MURI 'Fundamental Mechanisms, Predictive Modeling, and Novel Aerospace Applications of Plasma Assisted Combustion' (Arlington, VA)*

[18] Dagaut P *et al* 1994 *25th Symp. (Int.) on Combustion (Irvine, CA)*

[19] Dagaut P, Bakali A E and Ristori A 2006 *Fuel* **85** 944

[20] Humer S *et al* 2007 *Proc. Combust. Inst.* **31** 393

[21] Balamuta J and Golde M F 1982 *J. Chem. Phys.* **76** 2430

[22] Balamuta J, Golde M F and Ho Y S 1983 *J. Chem. Phys.* **79** 2822

[23] Tsolas N, Togai K and Yetter R A 2015 *53rd AIAA Aerospace Sciences Meeting (Kissimmee, FL)*

[24] Malewicki T and Brezinsky K 2013 *Proc. Combust. Inst.* **34** 361

[25] Luo Y R 2007 *Comprehensive Handbook of Chemical Bond Energies* (Boca Raton, FL: CRC press)